

Processes controlling water vapor in the winter Arctic tropopause region

Leonhard Pfister,¹ Henry B. Selkirk,² Eric J. Jensen,¹ James Podolske,¹ Glen Sachse,⁴
Melody Avery,⁴ Mark R. Schoeberl,³ Michael J. Mahoney,⁵ and Erik Richard⁶

Received 9 July 2001; revised 18 January 2002; accepted 22 January 2002; published 7 December 2002.

[1] This work describes transport and thermodynamic processes that control water vapor near the tropopause during the SAGE III—Ozone Loss and Validation Experiment (SOLVE), held during the Arctic 1999/2000 winter season. Aircraft-based water vapor, carbon monoxide, and ozone measurements are analyzed so as to establish how deeply tropospheric air mixes into the Arctic lowermost stratosphere and what the implications are for cloud formation and water vapor removal in this region of the atmosphere. There are three major findings. First, troposphere-to-stratosphere exchange extends into the Arctic stratosphere to about 13 km. Penetration is to similar levels throughout the winter; however, because ozone increases with altitude most rapidly in the early spring, tropospheric air mixes with the highest values of ozone in that season. The effect of this upward mixing is to elevate water vapor mixing ratios significantly above their prevailing stratospheric values of about 5 ppmv. Second, the potential for cloud formation in the stratosphere is highest during early spring, with about 20% of the parcels which have ozone values of 300–350 ppbv experiencing ice saturation in a given 10 day period. Third, during early spring, temperatures at the tropopause are cold enough so that 5–10% of parcels experience relative humidities above 100%, even if the water content is as low as 5 ppmv. The implication is that during this period, dynamical processes near the Arctic tropopause can dehydrate air and keep the Arctic tropopause region very dry during early spring.

INDEX TERMS: 0368 Atmospheric Composition and Structure: Troposphere—constituent transport and chemistry; 0322 Atmospheric Composition and Structure: Constituent sources and sinks; 1655 Global Change: Water cycles (1836); 0320 Atmospheric Composition and Structure: Cloud physics and chemistry; 0341 Atmospheric Composition and Structure: Middle atmosphere—constituent transport and chemistry (3334); **KEYWORDS:** tropopause, water vapor, stratosphere-troposphere exchange, dehydration

Citation: Pfister, L., H. B. Selkirk, E. J. Jensen, J. Podolske, G. W. Sachse, M. A. Avery, M. R. Schoeberl, M. J. Mahoney, and E. Richard, Processes controlling water vapor in the winter Arctic tropopause region, *J. Geophys. Res.*, 107, 8314, doi:10.1029/2001JD001067, 2002. [printed 108(D5), 2003]

1. Introduction

[2] Water vapor in the winter Arctic tropopause region is important for two basic reasons. First, after the tropical tropopause region, the winter Arctic tropopause has the coldest temperatures in the tropospheric northern hemisphere. This suggests the potential for cloud formation that can remove water vapor from a part of the atmosphere where radiatively active gases (such as water) exert a disproportionate influence on the earth's radiation budget [Jensen *et al.*, 1996]. Though the limited number of

measurements indicate that the mixing ratio of water vapor in much of the lowermost stratosphere is low and fairly constant [see Hints *et al.*, 1998; Tuck *et al.*, 1997], values near the tropopause are higher and much more variable. Also, lidar studies show that cirrus cloud layers are found most often near the tropopause [e.g., Winker and Vaughan, 1994], with some aircraft studies (E. J. Jensen, personal communication, 2001) showing cloud just above the tropopause. Murphy *et al.* [1990], in their analysis of aircraft data in the winter Arctic, showed that ice saturation was not uncommon within 1 km of the tropopause. Given the overall downward motion near the middle- and high-latitude tropopause implied by negative diabatic heating rates, the presence of clouds in this region implies an ability to regulate water vapor in the upper 2 km of the troposphere.

[3] The second reason for the importance of water in the Arctic tropopause region arises from the work of Solomon *et al.* [1997], which suggested that cirrus clouds near the tropopause could enhance the conversion of chlorine reservoir species ($ClNO_3$ and HCl) into active, ozone destroying molecules (ClO). The strength of this mechanism is crit-

¹NASA/Ames Research Center, Moffett Field, California, USA.

²Space Physics Research Institute Center, Sunnyvale, California, USA.

³NASA/Goddard Space Flight Center, Greenbelt, Maryland, USA.

⁴NASA/Langley Research Center, Hampton, Virginia, USA.

⁵Jet Propulsion Laboratory, California Institute of Technology, Pasadena, California, USA.

⁶NOAA Aeronomy Laboratory, Boulder, Colorado, USA.

ically dependent on the ability of clouds to penetrate into the stratosphere since ozone and the chlorine reservoir species have minimal concentrations in the upper troposphere. The importance of this mechanism is a matter of controversy; recent work by *Smith et al.* [2001] indicates that this mechanism is absent at least in the midlatitude stratosphere.

[4] The recent SOLVE (SAGE III—Ozone Loss and Validation Experiment) experiment, with extensive DC-8 aircraft in situ measurements of water vapor and tracers with a variety of lifetimes, offers an excellent opportunity to examine the processes that govern the distribution of water near the tropopause during the winter high latitudes. Details of the experiment are described by *Newman and Harris* [2002]. Briefly, the experiment took place in three phases (early December, late January, and early March), covering the early winter, midwinter, and early spring periods of 1999/2000. Each period had about 8 DC-8 flights in the Arctic tropopause region. The bulk of the data was in the lowermost stratosphere, but with some penetrations into the upper troposphere.

[5] The purpose of this work is to examine the data from this experiment with an eye to three basic questions aimed at understanding what governs the water vapor in the winter Arctic tropopause region. First, how extensive is troposphere-to-stratosphere exchange during the winter season? In particular how deeply into the stratosphere does tropospheric “short term” influence extend? Short-term here means quasi-isentropic mixing on timescales of a few weeks. This is to be contrasted with tropospheric air that has entered at the tropical tropopause, mixed poleward isentropically, and descended diabatically, a process which typically takes several months [R. Spackman et al., 2001]. A related question involves the implications of this “short-term” exchange for the water distribution. Second, how often can clouds form in this region, and how deeply into the lowermost stratosphere can we expect clouds to extend? Third, what is the effect of these clouds on water in the tropopause region? To answer these questions, we will examine tracer-tracer relationships derived from the aircraft data, which can provide clear evidence of the nature of mixing processes. This will be coupled with trajectory analyses of the air parcels sampled by the aircraft. A sufficiently large sample of trajectories can allow two types of statistical analysis which can establish: (1) how often air from within the lowermost stratosphere has a tropospheric origin, and (2) how often that air becomes cold enough to either form a cloud or reach high relative humidities.

2. Meteorological and Compositional Background

[6] Figures 1a–1c show zonally and time averaged cross-sections of temperature and temperature standard deviation during the three phases of SOLVE in the tropopause region using the Medium Range Forecast Model (MRF), produced by the National Centers for Environmental Prediction (NCEP). The tropopause is indicated in the figures, being the line where potential vorticity is equal to 2 PVU. The plotted values were arrived at by spline interpolating the 6-hourly analyses in the vertical to produce data at approximately 200 m intervals and calculating the temperature zonal and time average, and the standard deviation there-

from, for each of the three phases. The temperature evolution through the winter shows that the coldest average temperatures near the tropopause were during the midwinter phase, with slightly warmer temperatures during early spring and significantly warmer temperatures during early winter. Temperature standard deviations are a maximum around 12–14 km at middle to high latitudes. These high temperature standard deviations are due to the variations in the polar front jet stream, and the storms that develop along it [*Shapiro et al.*, 1987]. Standard deviations increased monotonically through the winter season, with maxima about twice as large during early spring as in early winter. The combination of average temperatures that are close to their coldest of the season in the early spring, and the increased storm activity (with a resulting increase in temperature variance), suggests that the early spring is the most favorable time for cloud formation in the Arctic tropopause region. It is also possible that quasi-isentropic mixing of tropospheric air into the stratosphere is strongest during this period.

[7] To assess the extent of mixing of tropospheric air into the stratosphere in the winter Arctic and its effect on cloud formation in the tropopause region, we will examine the relationships of the tropospheric tracers CO and water vapor to a stratospheric tracer whose lifetime is long compared to the mixing processes of interest, namely ozone. Typically ozone has fairly complex chemistry. However, with only limited sunlight in the lowermost winter Arctic stratosphere, ozone lifetimes are typically longer than the few weeks associated with quasi-isentropic mixing. Ozone also has two advantages over some other more “traditional” long-lived trace gases such as nitrous oxide. First, because of its extensive observational history, it can be used with confidence to define the tropopause, with values below 80–100 ppbv being reliable indicators of tropospheric air [*Bethan et al.*, 1996]. Second, the importance of the *Solomon et al.* [1997] mechanism for cirrus processing and possible ozone reduction is related to the extent of cirrus in regions of significant ozone. Thus an assessment of relative humidity and clouds as a function of ozone is a more direct approach to this problem. In any case, relationships of ozone to both nitrous oxide and methane in the lowermost stratosphere probed by the DC-8 during SOLVE (not shown) were very linear, and showed only small changes through the winter season.

[8] Figures 2 and 3 show carbon monoxide and water plotted against ozone for each of the three phases of SOLVE. The individual flights are plotted in distinct colors. CO is from the DACOM tunable diode laser instrument [*Sachse et al.*, 1991], while water vapor is from an external path infrared laser hygrometer [*Vay et al.*, 2000]. Ozone is measured using a chemiluminescent technique [*Gregory et al.*, 1989]. Carbon monoxide is a tropospheric tracer that is moderately uniform in the troposphere (typically 80–120 ppbv outside of heavily polluted regions), with a lifetime of a few months in the stratosphere. Water is very nonuniform in the troposphere, due to extensive sources and sinks (cloud formation and evaporation). Most important, water is much more abundant in the troposphere than in the stratosphere, with a very strong vertical gradient below the tropopause (a typical mixing ratio scale height is 1.5 km, see [*Rind et al.*, 1993]). Thus even a fairly small fraction of tropospheric air within the stratosphere can be readily detected, at least

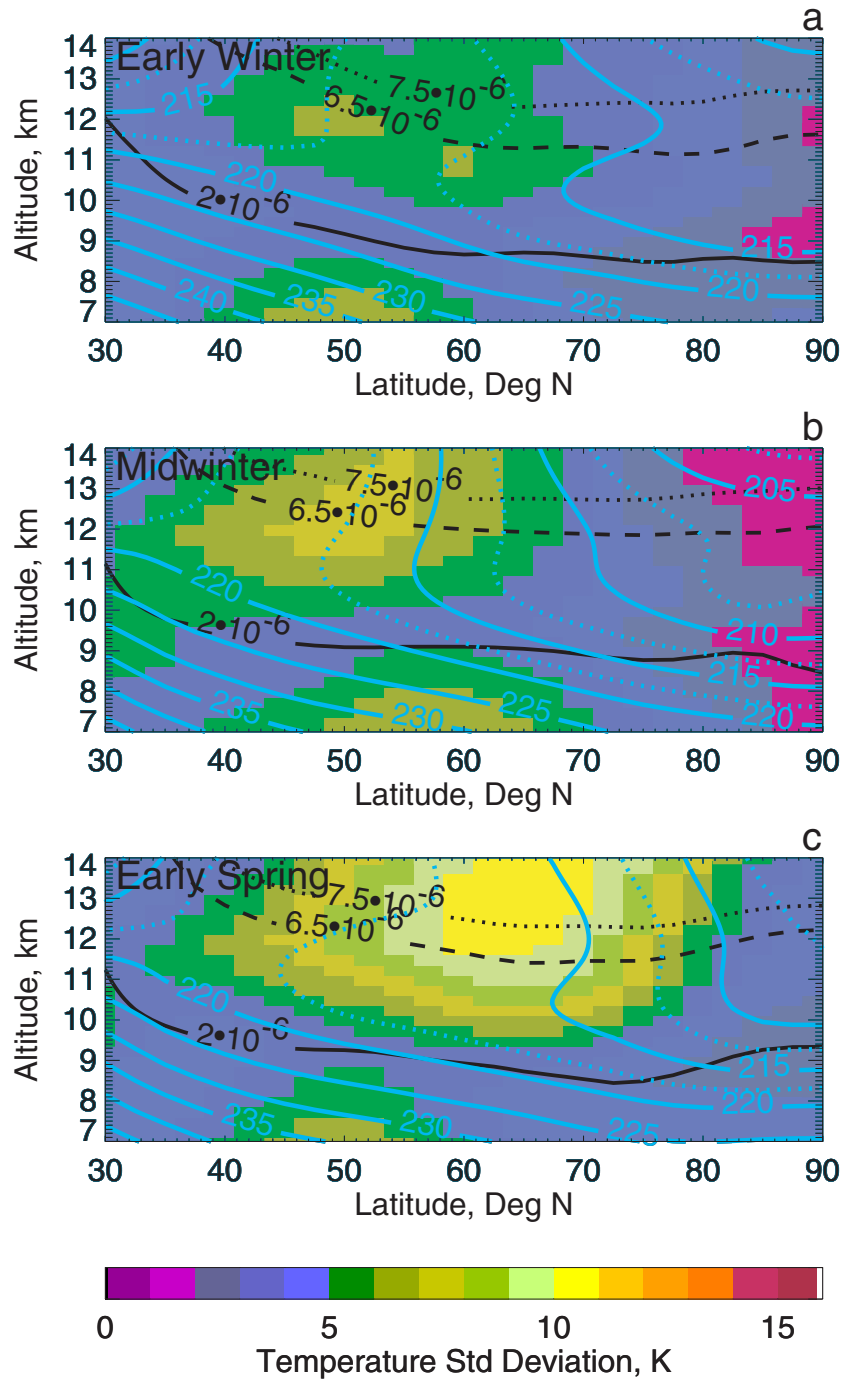


Figure 1. Zonally and time-averaged temperature and temperature standard deviations for the three deployment periods of SOLVE: (a) early winter (30 November 1999 to 16 December 1999); (b) midwinter (14–29 January 2000); and (c) early spring (27 February 2000 to 15 March 2000). Cyan contours are temperature, while the colored shading indicates the standard deviation. The tropopause, as defined by a potential vorticity of 2 PVU is denoted by the black solid line. The black dashed and dotted lines indicate potential vorticity surfaces to which tropospheric air penetrates, as described later in section 2.

qualitatively, by noting the water vapor. Water vapor content in the northern hemisphere stratosphere is largely determined by a combination of seasonally varying entry values at the tropical tropopause [Mote *et al.*, 1996], methane oxidation above 25 km, and some limited dehydration in the winter Arctic vortex [Herman *et al.*, 2002]. Thus variation is fairly small (compared to variation in the tropo-

sphere), being 4–6 ppmv in that part of the winter Arctic stratosphere not influenced by either isentropic mixing with the much moister troposphere [Dessler *et al.*, 1995] or convective injection [Poulida and Dickerson, 1996].

[9] As can be seen from Figure 2, the behavior of CO as a function of ozone is not linear throughout the ozone range, reflecting a relatively short lifetime in the stratosphere that

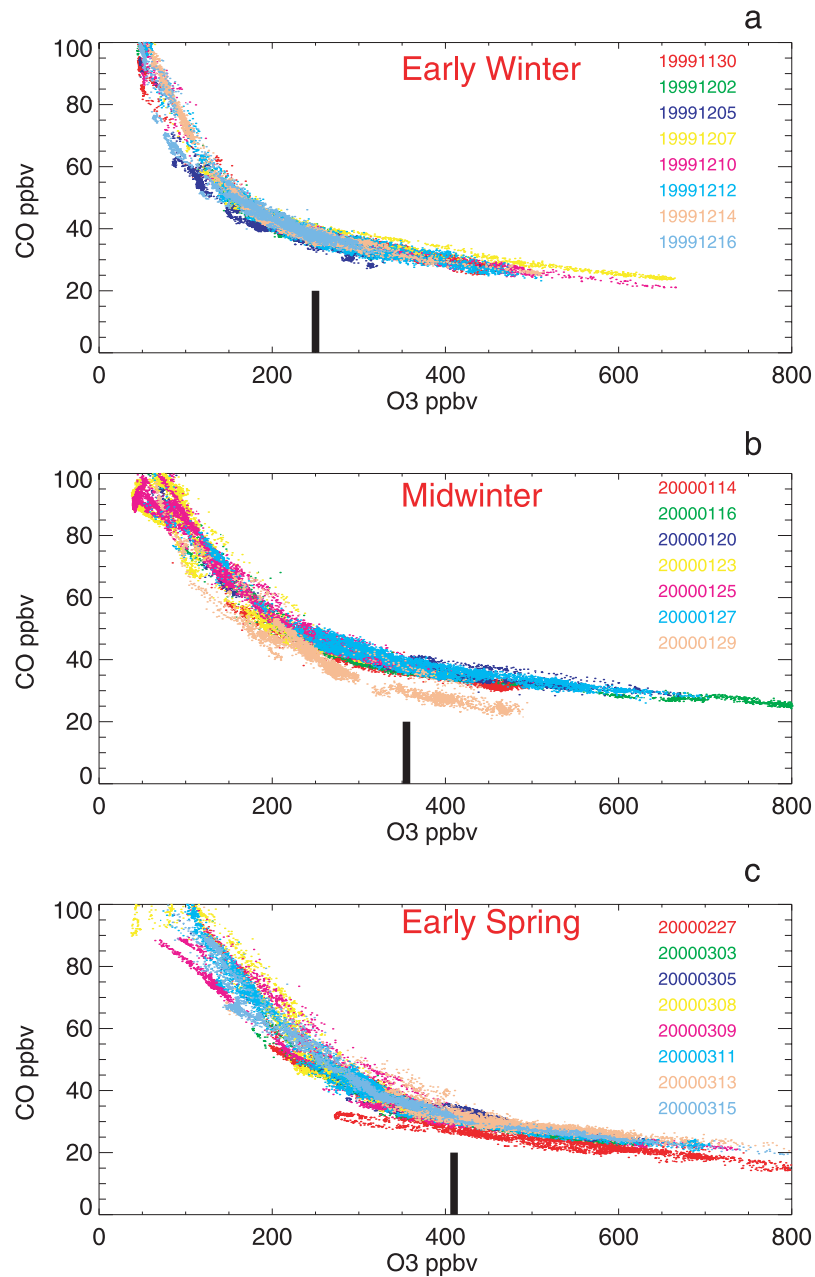


Figure 2. Carbon monoxide as a function of ozone on an individual flight basis for each of the three SOLVE deployments: (a) early winter, (b) midwinter, and (c) early spring. Heavy bars indicated the extent of apparent penetration of tropospheric air. Every fifth data point north of 55N is plotted.

suppresses its values below 30 ppbv. One feature of all the seasons is a small span of ozone values where the distribution changes from a fairly tightly packed flat exponential decay at high ozone to a curved, steeper character with a much bigger spread at lower ozone. This is most apparent in the early spring distribution, where a significant spread and change of slope develops below ozone values of about 410 ppbv. In fact, many individual flights exhibit a distinct “kink” in the distribution where there is an abrupt transition from a very gentle slope characteristic of the stratosphere to a steeper slope indicative of mixing with tropospheric air (e.g., 20000129 at 300 ppbv of ozone, 20000127 at 360 ppbv, 20000315 at 325 ppbv, 200001216 at 250 ppbv,

20000309 at 400 ppbv, and 20000313 at 410 ppbv). The steeper lines at values of ozone below this “kink point” slope between a point in the fairly tight distribution at higher ozone values and some tropospheric CO value between 80 and 130 ppbv. The implication is that there is significant and rapid (on timescales much less than the lifetime of CO) mixing with tropospheric air, rapid enough to exhibit a mixing line behavior. The spread in CO values below 250–400 ppbv ozone (depending on season) occurs both because of variability within the troposphere and the degree of penetration into the stratosphere of the mixing. Here degree of penetration is expressed in terms of the ozone value to which the in-mixing of tropospheric air

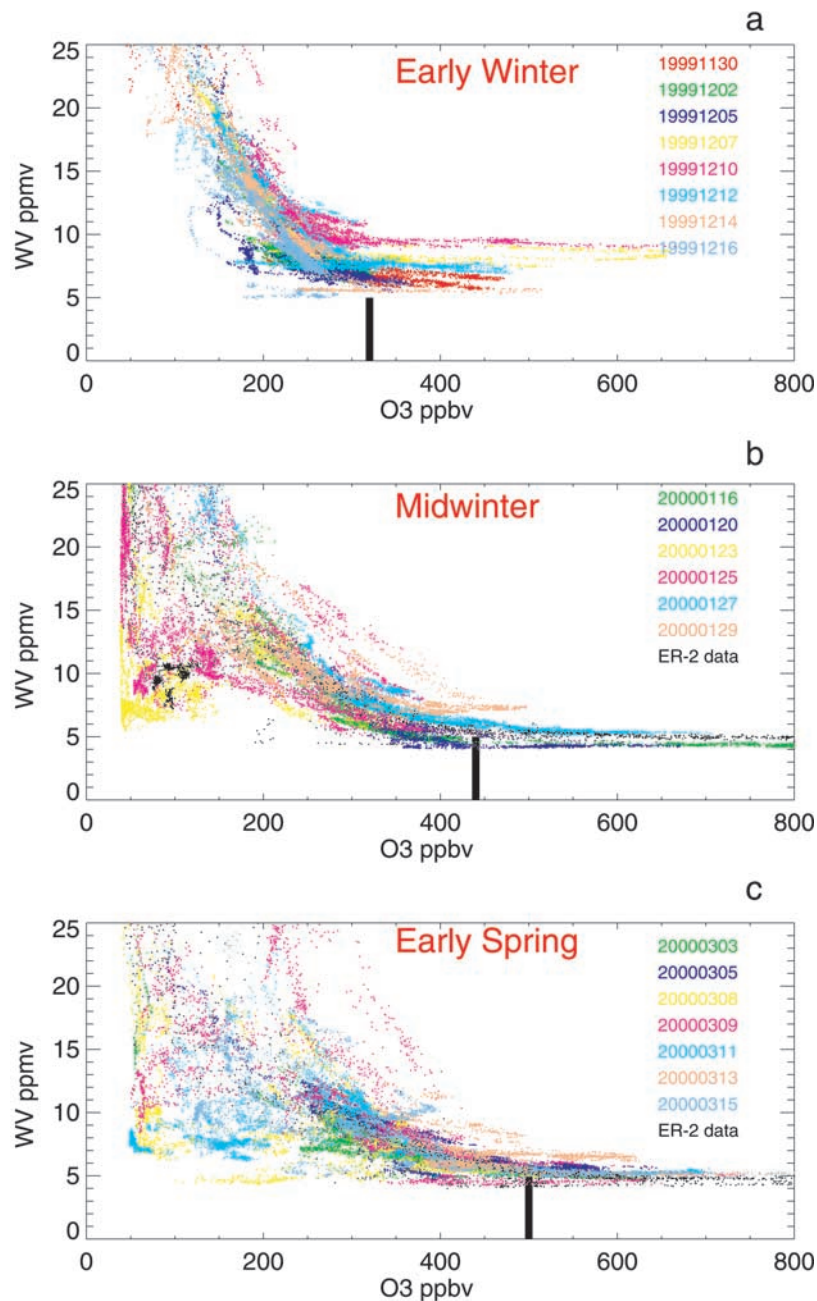


Figure 3. As in Figure 2, except for water vapor.

extends, which, as will be shown below, does not always imply the same degree of penetration in altitude. Notably, both the magnitude of the spread in the distributions at low ozone values and the degree of penetration into the stratosphere increase as the season progresses from early winter to early spring.

[10] The water traces (Figure 3) confirm this interpretation. For values of ozone above 300–500 ppbv (depending on the season), the distribution of water vapor forms a compact distribution at a nearly constant value (on an individual flight basis). Below these values of ozone, a significant spread develops, becoming very large as the tropopause (80–100 ppbv) is approached. This is presumably due to the variability of tropospheric sources. The

presence of large water vapor variability just above the tropopause has been in the meteorological literature for a long time [Ludlam, 1980]. Similar behavior was found by Hintsä et al. [1998], whose two case studies of mixing near the midlatitude tropopause showed markedly different mixing lines reflecting upper tropospheric variability in water. Another possible source for the spread is, of course, the possibility of clouds near the tropopause.

[11] It is clear that the penetration of rapid mixing with tropospheric air into higher ozone air in the lower stratosphere becomes greater as the seasons progress from early winter through early spring. This is apparent from both the ozone-CO relationship (Figure 2) and the ozone-water relationship (Figure 3). The values of ozone where the

distribution changes slope (for CO, Figure 2) or where the spread of values begins to increase (for water, Figure 3) are highlighted by the vertical black bars in the figures. For any given season, the water distribution suggests a deeper penetration of the mixing zone into the stratosphere than the CO distribution, which is not surprising since the very large differences between tropospheric and stratospheric values of water make it an indicator of small amounts of tropospheric air that could not be detected by the more modest differences between tropospheric and stratospheric CO. Also, water vapor has a much longer chemical lifetime than CO in the lowermost stratosphere.

[12] Figure 3 also includes water vapor measurements from the ER-2 aircraft [May, 1998], which flew similar flight tracks to the DC-8 (albeit generally at higher altitude) during the midwinter and early spring deployments. The data from this instrument shows reasonably good agreement with the DC-8 water measurements at high values of ozone (where we expect both measurements to asymptote to about 4–6 ppmv). The notable exceptions are the flight of 20000129, possibly the flight of 20000313 near 500–600 ppbv of ozone (though at 700 ppbv of ozone it is well within the range of the ER-2 measurements), and many of the flights of the early winter deployment. There is little evidence from limited previous measurements for water vapor above 6 ppmv at ozone values above 600 ppbv. The exceptions have been during late spring and summer, where there is evidence for convective injection in mid-latitudes to potential temperatures near 350 K and possibly higher [Poulida and Dickerson, 1996], which is well within the stratosphere at midlatitudes. Unpublished ER-2 measurements at midlatitudes during the December, 1996 STRAT (Stratospheric Tracers of Atmospheric Transport) campaign suggest that the water enhancements associated with these injections have disappeared (presumably mixed out and descended) by this time. At this point, the issue of the origin of the high values of water above 600 ppbv of ozone remains unresolved. However, the implications for the rapid quasi-isentropic mechanism of mixing tropospheric air into the stratosphere is minimal since the issue for this problem is the location in ozone of significant deviations from the asymptote (which is well-mixed and presumably free of recent injections of highly variable tropospheric water). For cloud formation in the stratosphere, the values of water at high ozone are obviously more important. As will be shown below, however, temperature variability is the more important factor in cloud formation in the stratosphere. It turns out that temperatures near the tropopause (Figure 1) are too high in any case for any significant stratospheric cloud formation during the early winter period.

[13] The implication of these tracer relationships is that there is mixing with the troposphere on a timescale less than the lifetime of CO into the lowermost stratosphere. This mixing does have a fairly definite limit, varying from about 300 ppbv of ozone in the early winter, to 440 ppbv during midwinter, and up to 500 ppbv during early spring. So far, the mixing has been quantified as the ozone value to which tropospheric air (as measured by water or CO enhancements over stratospheric values) penetrates. One question is how this mixing translates into a geometric penetration depth into the stratosphere. This can be

addressed in two ways. First, we compare ozone to a similar quasi-conserved quantity that can actually be derived from routine meteorological data (and thus globally mapped), namely potential vorticity. A geometric penetration depth can then be derived by establishing the mean position of the potential vorticity value to which tropospheric air penetrates. Potential vorticity, not directly measured “in situ,” is derived by interpolating the flight track to global analyses. The second approach is to simply plot the distribution of water vapor measurements against altitude above the tropopause (analogous to the distribution of water vapor against ozone in Figure 3). Fortunately, there actually is an “in situ” measurement of tropopause altitude at the aircraft’s location from the Microwave Temperature Profiler [Denning *et al.*, 1989].

[14] Figure 4 reflects the first approach, showing the relationship between aircraft-measured ozone and potential vorticity. Here potential vorticity is spatially and temporally interpolated to the aircraft flight track from meteorological analyses. The relationship of potential vorticity and trace constituents in the lower stratosphere has been the subject of significant previous work [e.g., Tuck and Tao, 1994]. The significant amount of scatter reflects the fact that the aircraft captures the full spectrum of variation, while the potential vorticity reflects scales equal to or greater than the resolution of the model (in this case, 2.5°). One feature of Figure 4 is that, for potential vorticities above 2 PVU, the fitted cubic curves and the actual data for the three experimental periods begin to diverge. Though there is some fuzziness in the choice of potential vorticity values for the tropopause, it appears that the choice of 2 PVU, corresponding to an ozone value of 80 ppbv, is reasonable. 80 ppbv is also a reasonable choice based on ozonesonde data [Bethan *et al.*, 1996]. The second feature of the figure is that there is a notable evolution of the ozone on potential vorticity surfaces as the season progresses, with ozone effectively “flowing through” (downward) potential vorticity surfaces; alternatively stated, a given level of ozone reaches to lower potential vorticities later in the season. A thorough treatment of why this occurs is beyond the scope of this work. However, on a seasonal timescale of many months, neither ozone nor potential vorticity are truly conservative, so some shift is not surprising.

[15] The implication of this evolution for the depth of the “mixing zone” (at least as determined by this method), however, is clear. Though tropospheric air reaches higher ozone values as the season progresses, the value of potential vorticity to which tropospheric air penetrates, as well as the geometric depth of the mixing zone that this implies, remains about the same. Based on CO and water, tropospheric air penetrates to about 6.5 PVU (2.5–3.0 km above the PV/ozone tropopause) and 7.5 PVU (3.5–4.0 km above the PV/ozone tropopause), respectively, regardless of season; these two characteristic mixing depths are labelled in Figure 1. Notably, the resulting effective depth is similar to the 4 km depth above the tropopause where significant ice saturation was found by Murphy *et al.* [1990].

[16] Figure 5, showing the relationship between water vapor and the height above the tropopause, represents the second approach to establishing the mixing penetration depth. Here the height of the tropopause is measured every 10 s by comparing the altitude of the aircraft to the thermal

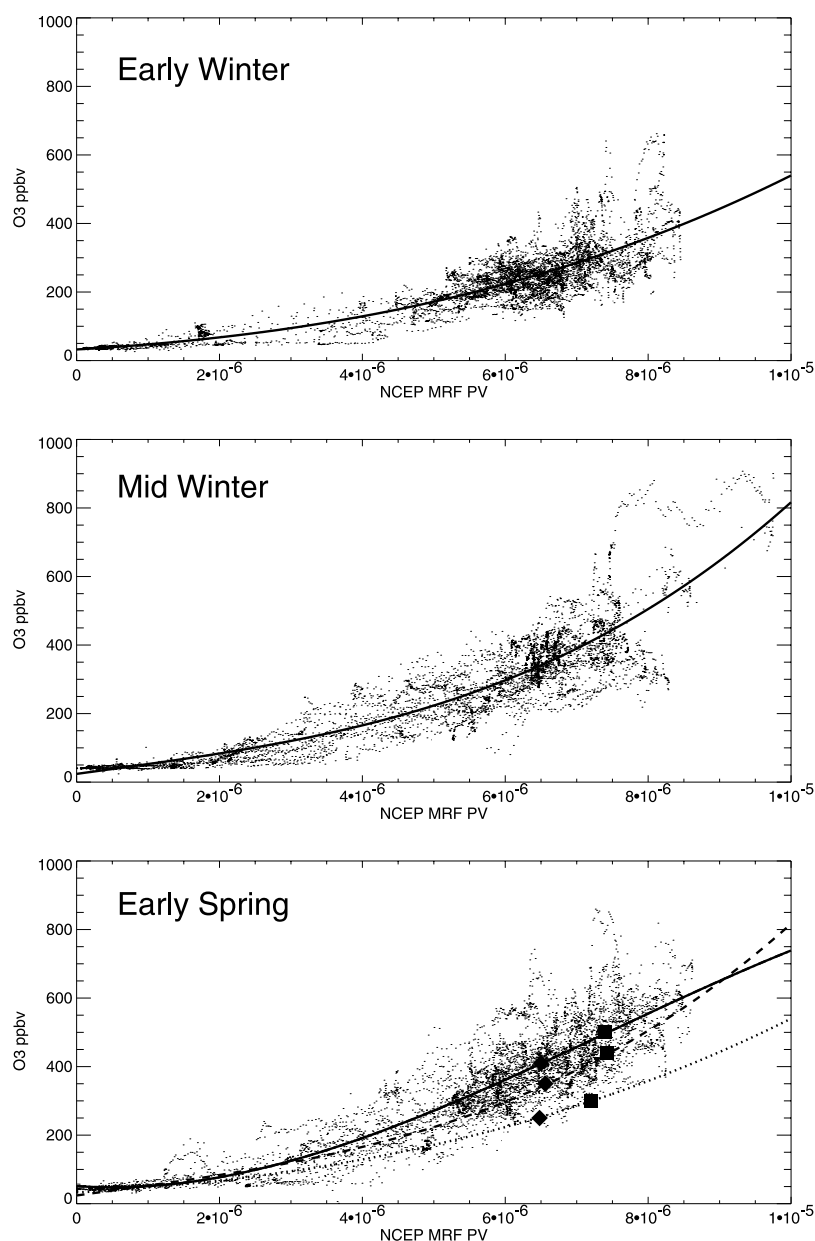


Figure 4. Ozone measured by aircraft as a function of NCEP MRF analysis potential vorticities (see text, section 2) for the three SOLVE deployments. The heavy solid lines are cubic least squares fits to the data points. The dotted and dashed curves in the early spring plot represent least squares cubic fits for the early and midwinter deployments, respectively. The filled squares in the early spring plot represent the mixing penetration based on water vapor measurements. The filled diamonds in the early spring plot represent the mixing penetration based on CO measurements.

tropopause as derived from a temperature profile measured by a remote microwave instrument on board the aircraft [Denning *et al.*, 1989]. Since water is nearly constant at about 4–6 ppmv in the stratosphere above the mixing zone, the altitude above the tropopause at which scatter is eliminated presumably represents the maximum geometric penetration of tropospheric air during each deployment. Using this approach, we arrive at geometric penetration depths above the thermal tropopause of 2.3, 1.8, and 1.9 km for the early winter, midwinter, and early spring deployments, respectively. Based on radiosonde comparisons [Bethan *et al.*, 1996], which showed that the thermal tropopause was

about 1 km above the ozone tropopause, this second method suggests a penetration depth of about 3 km above the PV/ozone tropopause. As with the potential vorticity method, the depths are comparable for all the seasons. The penetration depth is smaller than that derived using the PV method by 0.5–1 km. However, given the scatter in the potential vorticity (the 0.5–1 km distance is equivalent to about 1.0 PVU in Figure 4), this difference is probably not significant.

[17] One can speculate as to why this characteristic “mixing zone” retains the same depth in spite of the greater storm activity in the early spring season (as evidenced by

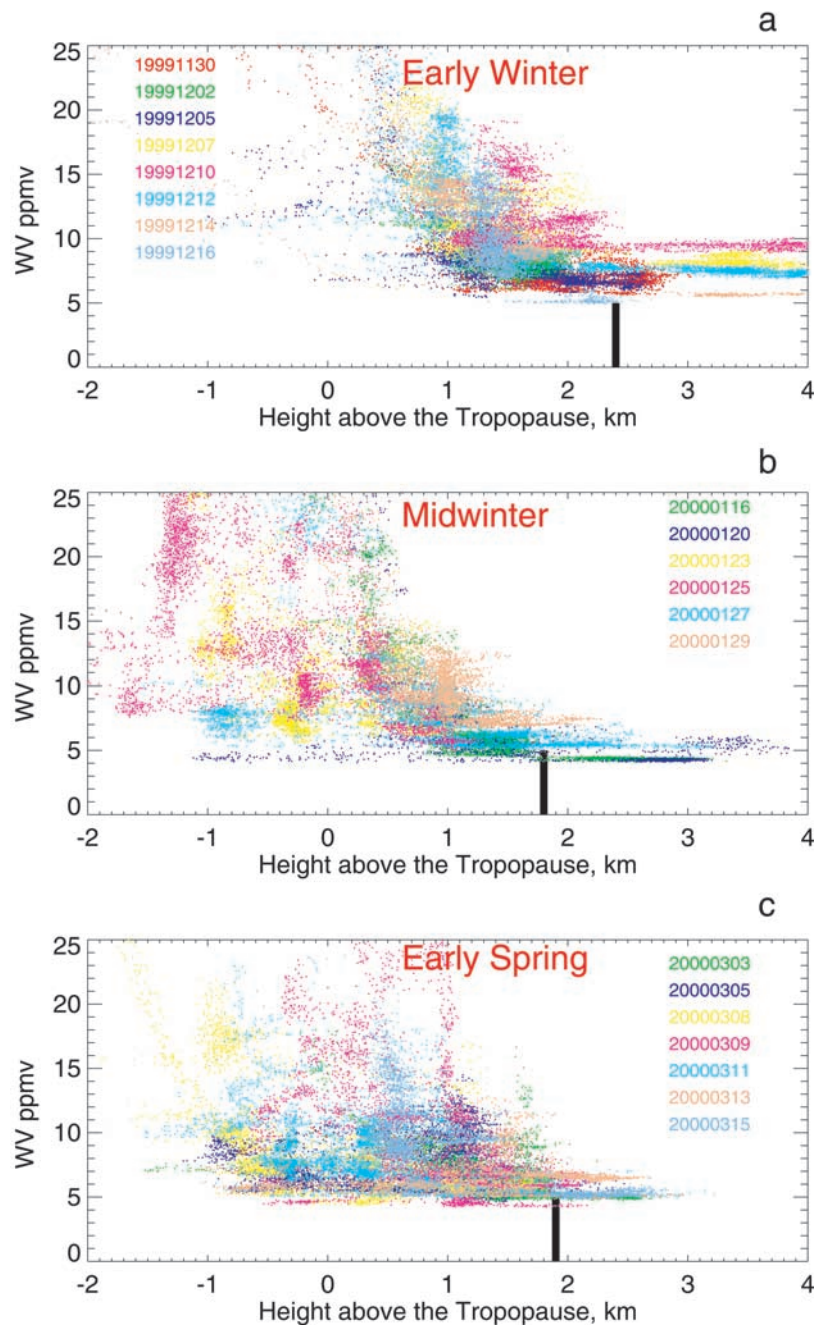


Figure 5. Water vapor as a function of height above the tropopause on an individual flight basis for each of the three SOLVE deployments. Heavy bars indicate the extent of apparent penetration of tropospheric air. Every fifth data point north of 55N is plotted.

the higher temperature variance in Figure 1). Upward mixing of tropospheric air is countered by mean, diabatically driven downward motion [Rosenlof, 1995]. Though this downward motion is strongest during the winter season, the actual net flow of air through the tropopause is strongest in the spring because the tropopause is actually moving upward during this period [Appenzeller *et al.*, 1996]. Thus, viewed from the perspective of the tropopause, the fairly constant depth of the mixing zone could be due to increased mixing in the spring counteracted by an increased downward cross-tropopause flow.

[18] Another important feature of the water vapor measurements, which is apparent in both Figures 3 and 5, concerns the values in the troposphere, that is, water vapor at values of ozone less than 80 ppbv. During early winter, tropospheric water vapor is generally quite high, with most of the tropospheric data points greater than the 25 ppmv maximum depicted in the figures. This changes as the season progresses, with a significant number of very dry observations within the troposphere. Figures 6a and 6b, which show the frequency distributions for both the upper troposphere within 2 km of the tropopause (Figure 6a), and

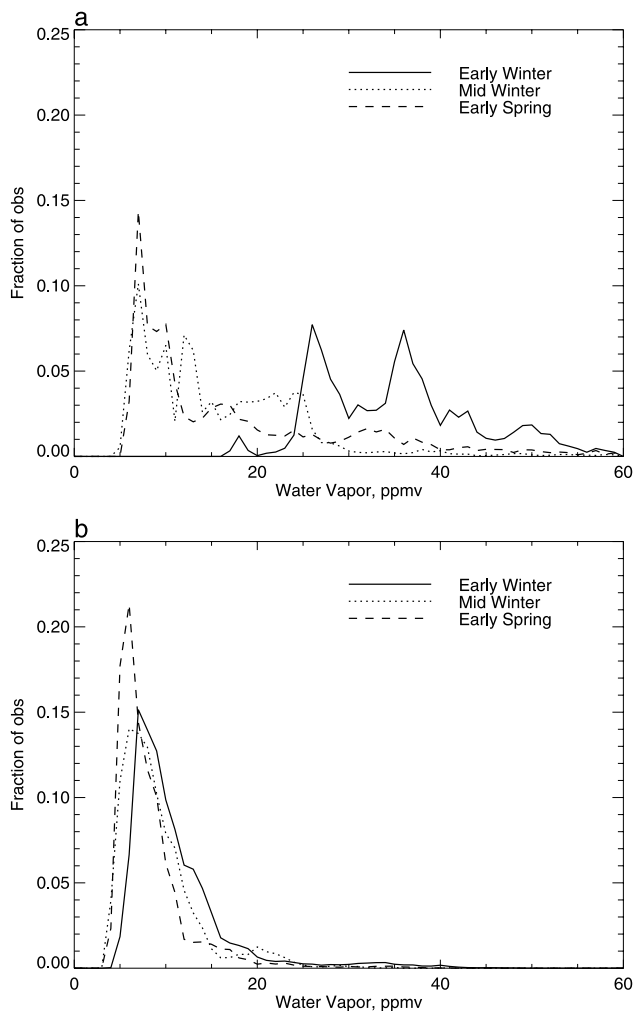


Figure 6. Frequency distribution of water vapor observations in 1 ppmv bins for the three deployments in (a) the troposphere (ozone less than 80 ppbv) and (b) the stratospheric mixing layer (ozone greater than 80 ppbv and less than the values for each deployment indicated by the heavy vertical bars in Figure 3).

the stratospheric mixing layer as determined by the tropopause and the respective vertical bars in Figure 5b (Figure 6b), show this trend clearly. In the upper 2 km of the troposphere, 98% of the observations in early winter are above 20 ppmv. This shifts dramatically and progressively through the season, so that by early spring, 33% are less than 10 ppmv. A qualitatively similar shift occurs in the stratospheric mixing layer, where the proportion of observations with values less than 10 ppmv increases from 50% in early winter to 78% in early spring. Notably, the frequency distributions go to zero near about 4 ppmv, which is consistent with the results of *Kelly et al.* [1991], who compared austral and boreal winter water vapor distributions near the tropopause. Much of this dry air in the uppermost troposphere could be due to downward transport of stratospheric air, which is consistent with the strengthening of the downward diabatic circulation during winter and spring [*Holton et al.*, 1995]. However, there are a significant number of points with water vapor very close to strato-

spheric values (less than 7 ppmv) with clearly tropospheric ozone values (50 ppbv). Given ozone's long lifetime in this region, this implies that the tropospheric air with which the incoming stratospheric air has mixed must also be quite dry; alternatively, there may be a dehydration mechanism within the upper troposphere, presumably near the tropopause where tropospheric temperatures are coldest [*Kelly et al.*, 1991]. As will be shown below, the tropopause region in this area can become quite cold on occasion and is probably a source for much of this dry air.

[19] We turn now to answering two questions that are raised by the tracer evidence. These are: (1) can the mixing of tropospheric tracers upward into the stratosphere be explained by quasi-isentropic mixing due to synoptic-scale motions (motions that can be resolved by global analyses); and (2) what are the implications for possible cloud formation and dehydration in the Arctic winter tropopause region?

3. Trajectory Method and Approach

[20] Trajectory analysis is a useful approach to obtaining answers to both of these questions. For the first question, a statistical picture of the history of air parcels as a function of how "deep" the air parcel is in the stratosphere (as measured by ozone) can show the likelihood that the air parcel had a tropospheric origin. For the second question, a temperature history, coupled with the aircraft water vapor measurements, can show the likelihood that a cloud occurred in any given parcel's history (simply by looking for relative humidities greater than 100%). It should be noted that trajectory methods based on large scale analyses have their limitations. For the transport issue, trajectory analysis does not include processes such as turbulent mixing and lateral mixing by inertia-gravity waves [*Danielsen*, 1993]. For the cloud formation issue, small-scale gravity waves can have significant effects on the temperature [*Gary et al.*, 1989]. The conventional wisdom at this time is that turbulent mixing (except as the last stage of mixing distended tracer structures created by large-scale motions into the environment) is relatively unimportant. Small-scale gravity waves probably have sufficiently short timescales so that the particles formed are too small to fall out [*Jensen et al.*, 1996]. Nevertheless, it should be noted that there is no overwhelming assurance that turbulence, inertia-gravity waves, or conventional gravity waves can be ignored.

[21] The approach is to perform 10 day isentropic back trajectories [*Schoeberl and Sparling*, 1995] from points along the flight track, and then ask two questions. First, have these back trajectories encountered tropospheric air? Second, what is the history of relative humidity of the air parcels (based on temperature and observed water vapor)? Because it is computationally most efficient to calculate the trajectories in clusters that share a common potential temperature and a common starting time, each flight is divided into three or four 3-h segments. The points in these segments are then separated into 4° potential temperature bins between 302 and 396 K (2° bins between 302 and 310 K). The starting time for each potential temperature bin is the average of the observation times of all the points in that bin. Taking every thirtieth point in the time series, this yields about 1000 trajectories for each flight, divided into about 30

potential temperature/starting time clusters. Typically, this means we have 6000–8000 trajectories for each phase of SOLVE.

[22] The maximum potential temperature error due to this binning approach is 2 K, with the maximum timing error about 1.5 h. Since the analyses which are used to calculate the trajectories are 6 h apart, this timing error is deemed small compared to interpolation errors due to the time spacing of the analyses. The error due to binning by potential temperature comes in two forms, both forms related to errors in altitude implied by the 2 K error in potential temperature; essentially, one is calculating the trajectory at the “wrong” altitude. In the stratosphere, this implies an altitude error of about 200 m, or about one tenth of the vertical resolution of the analyses. The altitude error in the troposphere is similar (since we are using 2 K binning with a 1 K error at tropospheric potential temperatures). The implication of these errors is that wind errors due to the binning error (which govern the trajectory positions) should be substantially smaller than errors due to the analyses. Temperature errors in the stratosphere will be near zero (because the stratosphere is nearly isothermal); temperature errors in the troposphere will be larger (due to strong vertical temperature gradients), but still less than 1.5 K. Errors in the critical tropopause region will be less than a degree, which is similar to expected errors in the analyses.

[23] An important question is: which analysis is best for calculating the trajectories for this particular problem? This is critical for the issue of relative humidity, which is very sensitive to temperature. Analyses are produced using a combination of radiosonde observations, satellite observations, commercial aircraft observations, and the physical laws as implemented in complex three-dimensional models. Differences in analyses reflect differing models, and the judgments those models make about ensuring that the input data are physically self-consistent. Analyses can be compared to each other and to radiosonde and satellite data in an attempt to decide which one is the “best” for any particular purpose. The problem with this approach is its incestuous character since analyses are all derived from similar radiosonde and satellite data sets. The SOLVE mission presents an opportunity to compare temperature analyses with an extensive set of DC-8 aircraft measurements. Though far from global, it covers much of the Arctic tropopause region fairly well and the analyses can be said to be independent of this data set.

[24] Measuring temperature from aircraft, especially to the accuracies that are desirable for examining issues of ice saturation, is not a trivial undertaking [Gaines *et al.*, 1992]. Though published comparisons between the aircraft facility instrument on the DC-8 and radiosondes have not been made, some of the experimental groups aboard the DC-8 do monitor the radiosonde data regularly. One of them (M. J. Mahoney, personal communication, 2001) reports that the aircraft temperatures appear to be systematically warm (relative to radiosondes) by about .8 K. However, there is no evidence that this difference is anything other than a systematic bias. The expectation is that the aircraft data will provide better information on the atmospheric variations (in the limited regions where there is data), while perhaps systematically overestimating the temperatures by something less than 1 K.

[25] Figures 7a–7c shows comparisons between DC-8 aircraft temperatures in the tropopause region and three analysis products, the NCEP MRF, the NCEP reanalysis product, and the GEOS-1 assimilation model [Schubert and Rood, 1993]. Printed in each figure is the bias of the analysis data relative to the aircraft data, as well as the root mean squared (RMS) difference after the bias has been removed. To obtain the analysis information along the aircraft flight track, spatial spline interpolations to the flight track position were performed at the 6-hourly analysis times that were relevant for each particular flight. These interpolations were, in turn, linearly interpolated in time in accordance with the actual time that the aircraft data was taken.

[26] There are two points to note. First, the analyses are all colder, on the average, than the aircraft data. Though not as large as the .8 K noted above, this difference is qualitatively consistent with the unpublished comparisons with radiosondes. Second, it is clear that the NCEP MRF analysis is best able to capture the temperature variations in the tropopause region during this period, with substantially lower RMS differences than the other two analyses. In particular, the NMC reanalysis seems to have a “floor” of about 200.5 K, at least in the regions and times sampled by the aircraft. Based on this comparison, we will choose the MRF analysis product to perform the trajectory analyses. Note, however, that the NCEP MRF will produce the coldest temperatures, and the highest relative humidities of the three analysis products.

4. Results and Discussion

[27] The trajectory information is binned by ozone (as measured by the aircraft), where ozone is a reasonable indicator of how “stratospheric” the air is. Four quantities derived from the back trajectories from aircraft data are plotted. Figure 8a shows the percentage of trajectories that experience tropospheric potential vorticities at some time in their history, where tropospheric potential vorticity is defined as a PV of less than 2 PVU. Figure 8b (heavy lines) shows the percentage of aircraft-observed parcels with relative humidities greater than 100%, as derived from aircraft-observed temperature, pressure, and water vapor. The light lines show the same information, except using analysis temperature and aircraft-measured water. Figure 8c shows the percentage of aircraft-observed parcels that experienced relative humidities greater than 100% at some time in the past 10 days (based on aircraft-observed water vapor and temperatures and pressures along the back trajectory). Finally, Figure 8d shows the percentage of aircraft-observed parcels that have experienced ice saturation mixing ratios less than 5 ppmv sometime in the past 10 days.

[28] Examining Figure 8a, we find, not surprisingly, that those parcels near the tropopause (ozone values of less than 150 ppbv or so) experience tropospheric air quite frequently. Above 150 ppbv, the drop-off is quite sharp, reaching an insignificant fraction at between 250 and 375 ppbv (depending on season), which is the approximate location of the slope change in the CO trace in Figure 2. Notably, the drop-off is less steep and occurs at higher ozone values as the season progresses, consistent with the traces in Figure 2. The long term transport of PV is not able to explain the

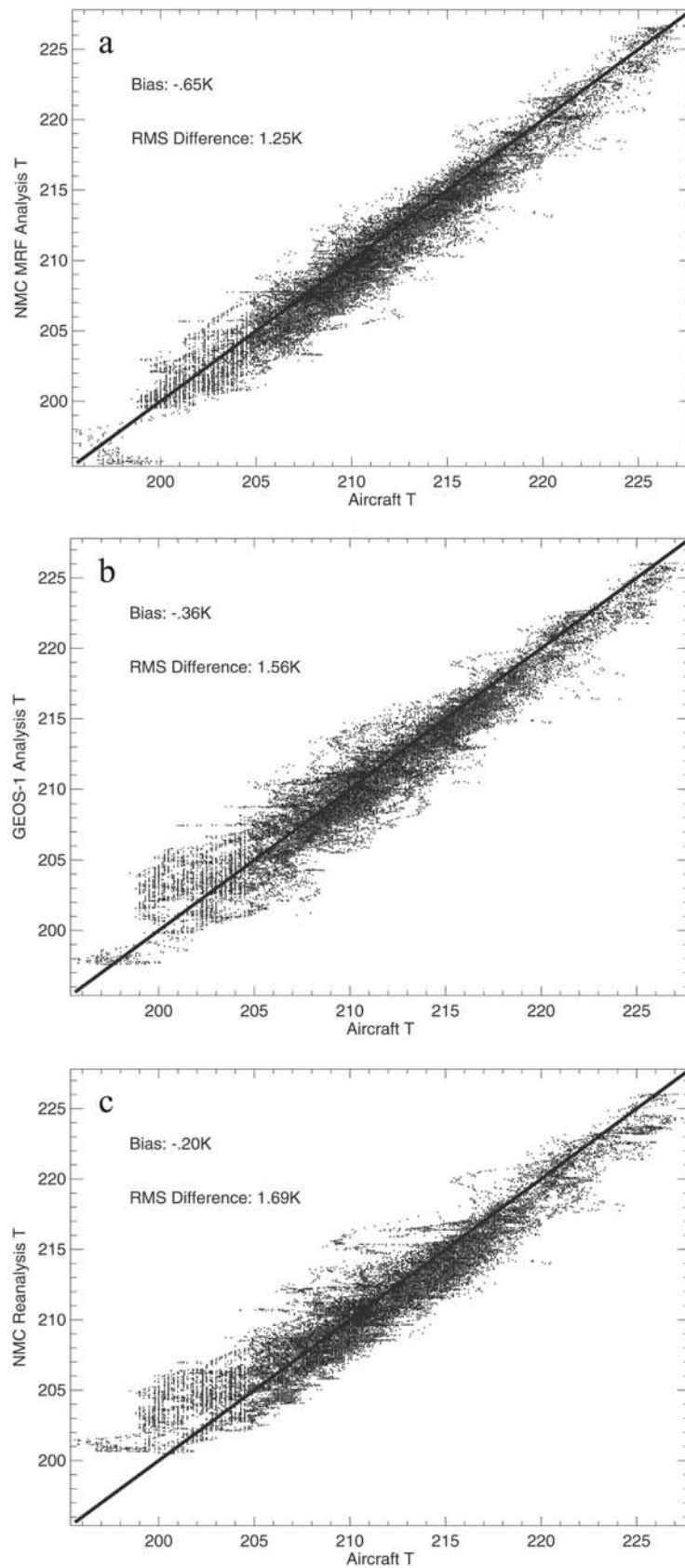


Figure 7. Analysis temperatures interpolated along the aircraft flight track plotted against aircraft measured temperatures for three different analysis products: (a) NCEP MRF analysis, (b) GEOS-1 analysis, and (c) NCEP reanalysis. The heavy solid line is the line of equal temperatures.

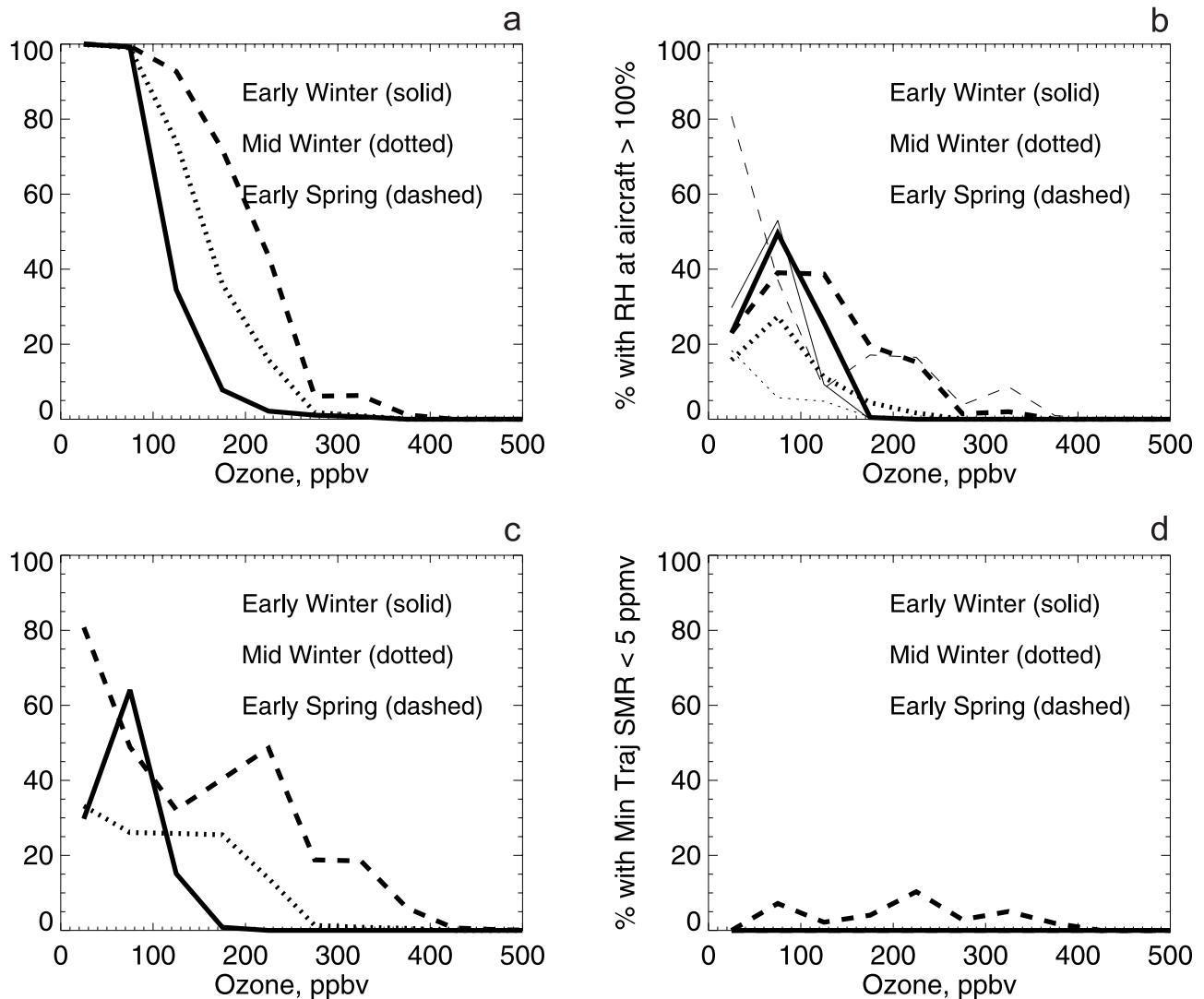


Figure 8. Results of trajectory analyses binned by aircraft-observed ozone for the early winter period (solid), midwinter period (dotted) and early spring period (dashed). (a) Percentage of parcels with tropospheric potential vorticities (less than 2 PVU) in their 10 day history. (b) Percentage of parcels having a relative humidity at the observation time that is greater than 100% (heavy lines denote the use of aircraft temperatures, light lines denote the use of analysis temperatures). (c) Percentage of parcels that had relative humidity greater than 100% sometime in their 10 day trajectory history. (d) Percentage of parcels that experience saturation mixing ratios less than 5 ppmv sometime in their 10 day trajectory history.

extent of penetration exhibited in the water data in Figure 3. It is possible that the water vapor enhancements over the stratospheric value are due not to direct in-mixing of tropospheric air, but mixing of air from the “edge region” around the tropopause (which has enhanced water vapor due to previous mixing events). In other words, the 10 day trajectory period may well be too short.

[29] Figures 8b and 8c examine the relative humidity for all the aircraft-observed parcels, first at the observation time (Figure 8b), and then during the 10 day trajectory history (Figure 8c). They show, binned by ozone, the percentage of parcels experiencing relative humidities of 100% or greater at the observation time (Figure 8b) or at some time during the 10 day history of the observed parcels (Figure 8c). Two features are to be noted. First, the relative humidity statistics for analysis and observed temperatures in Figure 8b

are at least in crude agreement, which reinforces the use of NCEP MRF analysis for this particular purpose. The large difference in the lowest ozone bin (0–50 ppbv) is probably due to the limited sampling at that level of ozone. The difference at 300–350 ppbv of ozone during early spring is due to the fact that the analysis is significantly colder than the aircraft measurements during part of the flight of March 8, 2000, where the aircraft passed through a cloud within the stratosphere (though the coldest analysis temperatures on this flight were not colder than the coldest aircraft temperatures). Second, when the trajectory histories are included, the probability of relative humidities exceeding 100% increases, a result that should not be surprising. Essentially, the probability of a parcel exceeding 100% humidity some time in the previous 10 days is about two to four times as large as the probability at any given time.

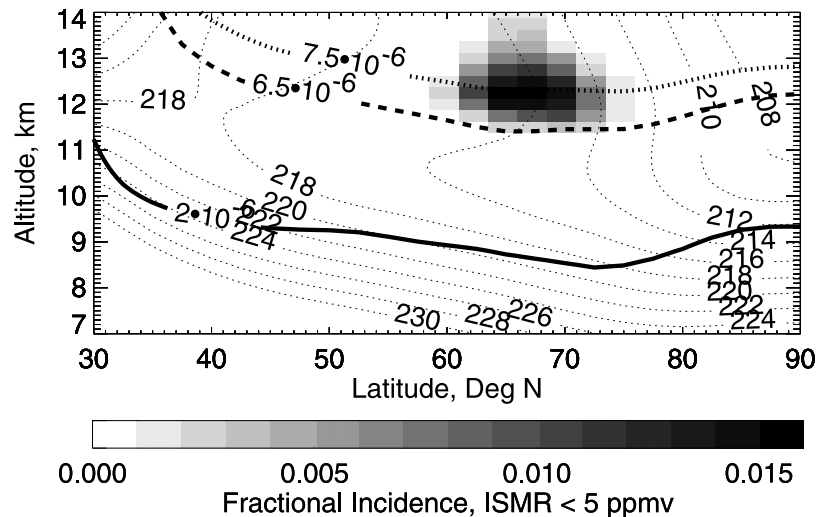


Figure 9. Fractional incidence of saturation mixing ratios less than 5 ppmv during the early spring period as a function of latitude and altitude. Gray scale denotes the fractional incidence and the light dotted lines are zonally and temporally averaged temperature contours. The heavy lines are potential vorticity contours, with the solid line denoting the tropopause and the dashed and dotted lines denoting the approximate upper limits of the mixing zone discussed in section 2 of the text.

Also, nonzero incidence of ice saturation is extended to higher values of ozone if the parcel histories are included; for early spring at 375 ppbv of ozone, the probability increases from near zero to about 7% when the 10 day history is included. Figures 8b and 8c also show that ice saturation does not appear to extend into the unmixed stratosphere in any season, namely the region shown in Figure 3 to the right of the heavy bars where water is nearly constant at 4–6 ppmv.

[30] It should be noted that the high unmixed stratospheric background water during early winter has no bearing on the incidence of ice saturation. For early winter, there are no instances of saturation, either in the data or in the history, above 125 ppbv of ozone, which is well below the unmixed stratospheric background that starts at 320 ppbv.

[31] An obvious feature of Figure 8 is the marked difference between the three phases of the 1999/2000 winter. Examining Figure 8c, we note that the drop-off in the probability of cloud along the trajectories occurs at higher values of ozone as the season progresses. The change in the ozone value of this drop-off is much larger than the corresponding change for the probability of tropospheric injection shown in Figure 8a. Essentially, tropospheric air penetrates to lower values of ozone in early winter, yet the incidence of clouds is even smaller, reflecting the higher temperatures in early winter. The same is due to a lesser extent for the comparison of midwinter to early spring. Notably, in comparing Figures 8b and 8c, the incidence of relative humidities greater than 100%, both along the trajectories and at the time of observation, is much larger in early winter than in midwinter at tropospheric values of ozone. This is due to the fact that water values are higher in early winter (Figure 3), making it easier to attain saturation. Overall, the incidences of relative humidities exceeding 100% are quite high (though it should be noted that the aircraft spent most of its time at ozone values above 300 ppbv, so one should not construe Figure 8b as an argument that the aircraft was in cloud 20–40% of the time). Clouds

may not always form when relative humidities reach 100%. In fact, recent laboratory work by [Koop *et al.*, 1998] indicates that significant ice supersaturation may be required for the formation of clouds. Also, E. J. Jensen (personal communication, 2001) has found incidences of supersaturation without evidence of clouds in a number of aircraft data sets.

[32] The above results indicate that potential cloud formation could affect the water distribution and, possibly, the chemistry well into the lowermost stratosphere, though there is no evidence of cloud formation above the top of the mixing region at 300–500 ppbv of ozone. Another question involves the potential ability of the temperature dynamics in the winter Arctic tropopause region to dehydrate air to very low values, such as the 5–7 ppmv seen between 50 and 150 ppbv of ozone on the flights of 20000308 and 20000311 (Figure 3). We thus pose the question as to how frequently air having 5 ppmv of water could become saturated. Figure 8d shows the percentage of trajectories with minimum saturation mixing ratios in the past 10 days of 5 ppmv or less. The results suggest that between 5 and 10% of the parcels in the tropopause region encounter such values during the early spring period, with no such cases for the early winter and midwinter periods.

[33] This finding is consistent with the results of Figures 9 and 10, which show two ways of displaying the incidence of ice saturation mixing ratios less than 5 ppmv during the early spring period of SOLVE. For Figure 9, NCEP MRF analysis data was spline interpolated at 200 m intervals in the vertical, and the incidence of ice saturation less than 5 ppmv calculated as a function of altitude and latitude. The results show a maximum occurrence during early spring between 60 and 80N and 11–14 km altitude. This is consistent with Figure 1, where the combination of high temperature variance and cold mean temperatures appear favorable for incidences of the very cold temperatures (about 197 K at 11.5 km). It is also consistent with the

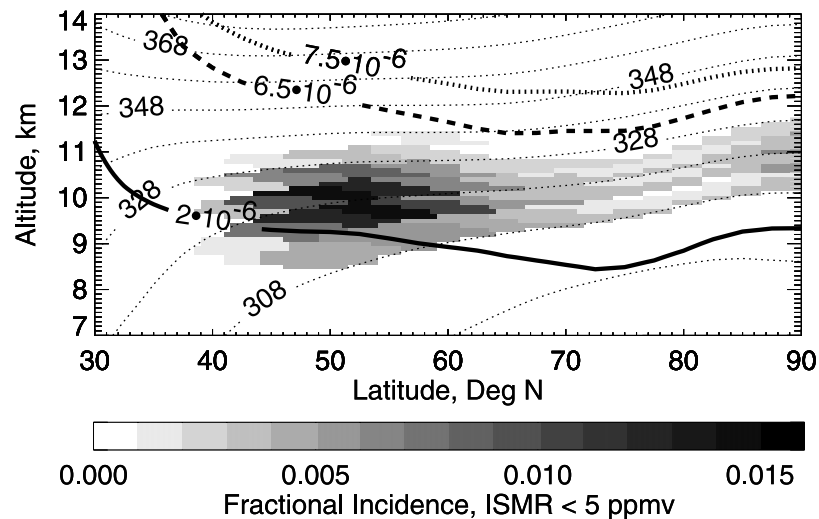


Figure 10. As in Figure 9, except that the incidences are binned by potential vorticity and potential temperature and plotted at the zonally and temporally averaged locations of those potential vorticities and potential temperatures. The temperature contours have been replaced by potential temperature contours. See text, section 4, for details.

aircraft observations of high relative humidities and low (4–5 ppmv) water vapor mixing ratios on March 8, observations which were made near 70N and 12 km altitude. Figure 9 suggests that dehydration and cloud formation occurs well inside the stratosphere, which, based on Figure 8c, is clearly not the case. Figure 10 shows the same data, but displayed in a different way. For Figure 10, NCEP MRF analysis data is again interpolated to 200 m intervals, and incidences of ice saturation mixing ratios less than 5 ppmv are calculated. However, these incidences are binned by potential vorticity and potential temperature. The incidences are then displayed on the mean cross-sections of potential vorticity and potential temperature for each period. The objective here is to isolate the air masses (as characterized by the quasi-conservative properties of potential vorticity and potential temperature) that experience low ice saturation mixing ratios, and locate their mean position in latitude-altitude space. Figure 10 shows that the air masses that experience low ice saturation mixing ratios are actually quite close to the tropopause, with a significant incidence below the tropopause (as clearly implied by Figure 8d). The mean position of these parcels is not 11–14 km and 60–80N (Figure 9), but 9–11 km and 40–60N.

[34] Two points arise from Figures 9 and 10. First, the incidence of ice saturation less than 5 ppmv along the trajectories during early spring (Figure 8d, about 5–10%) is clearly greater than the maximum overall incidence in Figures 9 and 10 (about 1.5%). The implication is that limited regions of very cold temperatures can affect a significant air mass due to the flow of air through those limited regions. The second point demonstrates, in a bulk sense, what the mechanism of cloud formation and dehydration in the winter Arctic tropopause region is. Namely, parcels whose mean positions are just poleward and above the mean tropospheric jet (30N) are moved upward and poleward, cooling in the process, forming clouds, and dehydrating. This process was clearly documented for the Antarctic spring by Kelly *et al.* [1991], who showed several

examples of parcels moving poleward from latitudes as low as 45S to the south pole, with pressures decreasing from 500 to 250 mb. These events were accompanied by extensive cloud shields seen in meteorological satellite data. They also showed extensive regions of dry air in the upper troposphere (defined as the region near 250 mb), with values as low as 2 ppmv in the Antarctic, and 4 ppmv in the Arctic. The same process of upward and poleward motion is occurring during the SOLVE mission, as demonstrated in the bulk sense by Figures 9 and 10, and shown by the March 8 case referred to above. In this case, the incidences of low (4–5 ppmv) values of water vapor can be traced back to latitudes between 20N and 50N and pressures as high as 400–500 mb. The aircraft-observed relative humidities for these 4–5 ppmv parcels is 80–90%, with nearby parcels with mixing ratios of 7–8 ppmv having relative humidities exceeding 100% (with clear evidence of cloud in the aircraft data).

5. Summary

[35] This work has investigated the processes governing water vapor in the winter Arctic tropopause region using a combination of trace gas analysis and trajectory analysis. The major findings are: (1) rapid (less than a month) timescale troposphere-to-stratosphere exchange extends into the stratosphere to levels where the ozone is about 300–500 ppbv, with significantly greater penetration during early spring and midwinter than in early winter. This is confirmed by trajectory analysis, which shows a very similar trend in the incidence of stratospheric parcels with tropospheric origins (as defined by potential vorticity). Notably, because the relationship of ozone to potential vorticity changes as the season progresses, the effective depth of mixing is about 2.5 to 3.5 km throughout the winter season. (2) the potential for cloud formation in the stratosphere is highest in early spring, with about 20% of parcels having ozone values of 300–350 ppbv experiencing ice saturation in their most

recent 10 day history. There is no evidence for cloud formation in that part of the stratosphere which does not have enhanced water above prevailing 4–6 ppmv values due to upward mixing from the troposphere. (3) Near the tropopause, there is a significant incidence of along-trajectory ice saturation mixing ratios below 5 ppmv. The process leading to this ice saturation at such low mixing ratios is due to large temperature excursions from the mean, due to synoptic storms. These storms take parcels whose mean position is just poleward of the tropospheric jet and lift them upward and poleward where cooling, cloud formation, and dehydration can take place.

[36] **Acknowledgments.** This work was funded by NASA's Upper Atmosphere Research Program. ER-2 water vapor measurements are courtesy of R. Herman of the Jet Propulsion Laboratory, California Institute of Technology, who carried out the work under contract with the National Aeronautics and Space Administration. Work by M. J. Mahoney at the Jet Propulsion Laboratory, California Institute of Technology, was carried out under contract with the National Aeronautics and Space Administration.

References

- Appenzeller, C., J. R. Holton, and K. H. Rosenlof, Seasonal variation of mass transport across the tropopause, *J. Geophys. Res.*, *101*, 15,071–15,078, 1996.
- Bethan, S., G. Vaughan, and S. J. Reid, A comparison of ozone and thermal tropopause heights and the impact of tropopause definition on quantifying the ozone content of the troposphere, *Q. J. R. Meteorol. Soc.*, *122*, 929–944, 1996.
- Danielsen, E. F., Irreversible transport in the stratosphere by internal waves of short vertical wavelength, *J. Geophys. Res.*, *96*, 17,433–17,452, 1993.
- Denning, R. F., S. L. Guidero, G. S. Parks, and B. L. Gary, Instrument description of the airborne microwave temperature profiler, *J. Geophys. Res.*, *94*, 16,757–16,765, 1989.
- Dessler, A. E., E. J. Hints, E. M. Weinstock, J. G. Anderson, and K. R. Chan, Mechanisms controlling water vapor in the lower stratosphere: “A Tale of Two Stratospheres”, *J. Geophys. Res.*, *100*, 23,167–23,172, 1995.
- Gaines, S. E., S. W. Bowen, R. S. Hipskind, T. P. Bui, and K. R. Chan, Comparisons of the NASA ER-2 meteorological measurement system with radar tracking and radiosonde data, *J. Atmos. Oceanic Technol.*, *9*, 210–225, 1992.
- Gary, B., Observational results using the microwave temperature profiler during the Airborne Antarctic Ozone Experiment, *J. Geophys. Res.*, *94*, 11,223–11,231, 1989.
- Gregory, G. L., W. D. Hypes, L. S. Warren, A. F. Tuck, K. K. Kelly, and A. J. Krueger, Tropospheric ozone in the vicinity of the ozone hole: 1987 Airborne Antarctic Ozone Experiment, *J. Geophys. Res.*, *94*, 16,537–16,547, 1989.
- Herman, R. L., et al., Hydration, dehydration, and the total hydrogen budget of the 1999/2000 winter Arctic stratosphere, *J. Geophys. Res.*, *107*, doi:10.1029/2001JD001257, in press, 2002.
- Hints, E. J., et al., Troposphere-to-stratosphere transport in the lowermost stratosphere from measurements of H_2O , CO_2 , N_2O , and O_3 , *Geophys. Res. Lett.*, *25*, 2655–2658, 1998.
- Holton, J. R., P. H. Haynes, M. E. McIntyre, A. R. Douglass, R. B. Rood, and L. Pfister, Stratosphere-troposphere exchange, *Rev. Geophys.*, *33*, 403–439, 1995.
- Jensen, E. J., O. B. Toon, L. Pfister, and H. B. Selkirk, Dehydration of the upper troposphere and lower stratosphere by subvisible cirrus clouds near the tropical tropopause, *Geophys. Res. Lett.*, *23*, 825–828, 1996.
- Kelly, K. K., A. F. Tuck, and T. Davies, Wintertime asymmetry of upper tropospheric water between the Northern and Southern Hemispheres, *Nature*, *353*, 244–247, 1991.
- Koop, T., H. P. Ng, L. T. Molina, and M. J. Molina, A new optical technique to study aerosol phase transitions: The nucleation of ice from H_2SO_4 aerosols, *J. Phys. Chem.*, *102*, 8924–8930, 1998.
- Ludlam, F. H., *Clouds and Storms*, 348 pp., Penn. State Univ. Press, University Park, Penn., 1980.
- May, R. D., Open-path, near-infrared tunable diode laser spectrometer for atmospheric measurements of H_2O , *J. Geophys. Res.*, *103*, 19,161–19,172, 1998.
- Mote, P. W., et al., An atmospheric tape recorder: The imprint of tropical tropopause temperatures on stratospheric water vapor, *J. Geophys. Res.*, *101*, 3989–4006, 1996.
- Murphy, D. M., K. K. Kelly, A. F. Tuck, and M. H. Proffitt, Ice saturation at the tropopause observed from ER-2 aircraft, *Geophys. Res. Lett.*, *17*, 353–356, 1990.
- Newman, P., et al., An overview of the SOLVE/THESEO 2000 campaign, *J. Geophys. Res.*, *107*, doi:10.1029/2001JD001303, in press, 2002.
- Pouliida, O., and R. R. Dickerson, Stratosphere-troposphere exchange in a midlatitude mesoscale convective complex, 1, Observations, *J. Geophys. Res.*, *101*, 6823–6836, 1996.
- Rind, D., E.-W. Chiou, W. Chu, S. Oltmans, J. Lerner, J. Larsen, M. P. McCormick, and L. McMaster, Overview of the Stratospheric Aerosol and Gas Experiment II water vapor observations: Method, validation, and data characteristics, *J. Geophys. Res.*, *98*, 4835–4856, 1993.
- Rosenlof, K., Seasonal cycle of the residual mean meridional circulation in the stratosphere, *J. Geophys. Res.*, *100*, 5173–5191, 1995.
- Sachse, G. W., J. E. Collins, Jr., G. R. Hill, L. O. Wade, L. G. Burney, and J. A. Ritter, Airborne tunable diode laser sensor for high-precision concentration and flux measurements of carbon monoxide and methane, in *Measurements of Atmospheric Gases*, Proc. SPIE, 1433, edited by H. I. Schiff, pp. 145–156, SPIE, Bellingham, Wash., 1991.
- Schoeberl, M., and L. C. Sparling, Trajectory modeling, in *Diagnostic Tools in Atmospheric Science*, Proc. Int. Sch. Phys. Enrico Fermi, *124*, 289–305, 1995.
- Schubert, S. D., and R. Rood, An assimilated data set for Earth science applications, *Am. Meteorol. Soc.*, *74*, 2331–2342, 1993.
- Shapiro, M. A., T. Hampel, and A. J. Krueger, The Arctic tropopause fold, *Mon. Weather Rev.*, *115*, 444–454, 1987.
- Smith, J. B., E. J. Hints, N. T. Allen, R. M. Stimpfle, and J. Anderson, Mechanisms for midlatitude ozone loss: Heterogeneous chemistry in the lowermost stratosphere?, *J. Geophys. Res.*, *106*, 1297–1309, 2001.
- Solomon, S., S. Borrmann, R. R. Garcia, R. Portmann, L. W. Thomason, L. R. Poole, D. Winker, and M. P. McCormick, Heterogeneous chlorine chemistry in the tropopause region, *J. Geophys. Res.*, *102*, 21,411–21,429, 1997.
- Tuck, A. F., and X. Tao, On the distribution of cold air near the vortex edge in the lower stratosphere, *J. Geophys. Res.*, *99*, 3431–3450, 1994.
- Tuck, A. F., et al., The Brewer-Dobson circulation in the light of high altitude in situ aircraft observations, *Q. J. R. Meteorol. Soc.*, *123*, 1–69, 1997.
- Vay, S. A., et al., Tropospheric water vapor measurements over the North Atlantic during the Subsonic Assessment Ozone and Nitrogen Oxide Experiment (SONEX), *J. Geophys. Res.*, *105*, 3745–3756, 2000.
- Winker, D. M., and M. A. Vaughan, Vertical distribution of clouds over Hampton, Virginia, observed by lidar under the ECLIPS and FIRE ETO programs, *Atmos. Res.*, *34*, 117–133, 1994.
- M. Avery and G. Sachse, Chemistry and Dynamics Branch, NASA/Langley Research Center, MS 401A, Hampton, VA 23691-2199, USA. (G.Sachse@larc.nasa.gov; M.Avery@larc.nasa.gov)
- E. J. Jensen, Atmospheric Physics Branch, NASA/Ames Research Center, MS 245-4, Moffett Field, CA 94035-1000, USA. (ejensen@mail.arc.nasa.gov)
- M. J. Mahoney, Jet Propulsion Laboratory, 4800 Oak Grove Drive, M/S 246-101, Pasadena, CA 91109, USA. (mmahoney@pop.jpl.nasa.gov)
- L. Pfister and J. Podolske, Atmospheric Chemistry and Dynamics Branch, NASA/Ames Research Center, MS 245-5, Moffett Field, CA 94035-1000, USA. (pfister@telsci.arc.nasa.gov; jpodolske@mail.arc.nasa.gov)
- E. C. Richard, NOAA Aeronomy Laboratory, Boulder, CO 80303, USA. (richard@al.noaa.gov)
- M. R. Schoeberl, Code 910., NASA/Goddard Space Flight Center, MS 916.0, Greenbelt, MD 20771, USA. (schom@zephyr.gsfc.nasa.gov)
- H. B. Selkirk, Space Physics Research Institute, Sunnyvale, CA 94087, USA. (hselkirk@mail.arc.nasa.gov)